Journal of Colloid and Interface Science 433 (2014) 141–148

Contents lists available at ScienceDirect

Journal of Colloid and Interface Science

www.elsevier.com/locate/jcis

Self-assembled monolayers of mercaptobenzoic acid and magnetite nanoparticles as an efficient support for development of tuberculosis genosensor

Maurilia P. Costa [a], Cesar A.S. Andrade [b], Rosana A. Montenegro [c], Fabio L. Melo [c], Maria D.L. Oliveira [a,b,*]

[a] Programa de Pós-Graduação em Bioquímica e Fisiologia, Universidade Federal de Pernambuco, 50670-901 Recife, PE, Brazil
[b] Departamento de Bioquímica, Universidade Federal de Pernambuco, 50670-901 Recife, PE, Brazil
[c] Laboratório de Doenças Transmissíveis, Centro de Pesquisas Aggeu Magalhães, 50670-420 Recife, PE, Brazil

ARTICLE INFO

Article history:
Received 18 May 2014
Accepted 12 July 2014
Available online 30 July 2014

Keywords:
Biosensor
Tuberculosis
Nanoparticles
Electrochemical impedance spectroscopy
Cyclic voltammetry

ABSTRACT

In this work, a genosensor for the electrochemical detection of genomic DNA from *Mycobacterium tuberculosis* was developed. The biosensor is based on self-assembled monolayers of mercaptobenzoic acid (MBA) and magnetite nanoparticles (Fe_3O_4Nps) on bare gold electrode for immobilization of DNA probe. The aim of this work was the development of a platform based on cysteine-coated magnetic Fe_3O_4Nps linked via the carboxylate group from MBA to the work electrode surface and subsequently to the DNA probe. The probe–genome interaction was evaluated using a $[Fe(CN)_6]^{4-}/[Fe(CN)_6]^{3-}$ redox pair. Cyclic voltammetry (CV) and electrochemical impedance spectroscopy (EIS) were used to evaluate the bioelectrochemical behavior of the sensor. Atomic force microscopy images showed Fe_3O_4Nps immobilized across the electrode surface. The interaction of the sensor with different genome DNA concentrations resulted in changes in the charge transfer resistance, indicating a possible use for tuberculosis detection at low concentrations (detection limit of 6 ng μL^{-1}).

1. Introduction

Tuberculosis (TB) is a common infectious disease caused by *Mycobacterium tuberculosis* and is one of the most widespread causes of death from a single infectious agent. The World Health Organization estimates that millions of new cases are discovered every year, resulting in ~2.4 million of deaths. Conventional methods for TB diagnosis, such as bacteriological culture, radiographic methods, polymerase chain reaction, restriction fragment length polymorphism, immunoassays and southern hybridization techniques are expensive, time-consuming and laborious [1]. Diverse molecular methods have been developed for the direct identification of TB [2,3]. Due to the precedence of TB as an important public health issue and the spread of drug-resistant tuberculosis the development of a new and rapid method for diagnosis is crucial. TB is a worldwide public health problem which demands new methods for diagnosis that include portability, cost-efficiency, and the possibility for reuse. To overcome these limitations, electrochemical assays have been used to provide a simple, reliable, inexpensive, sensitive, and selective platform for the deoxyribonucleic acid (DNA) detection [4].

Electrochemical biosensors are based on the application of low AC voltage overlaid onto a DC bias potential for the sensing electrode, and the AC current obtained thereof in the steady state [5]. It is important to note that the applicability of electrochemical impedance spectroscopy (EIS) in the development of biodevices has been increasing [6–9]. EIS has become one of the most used techniques for the development of biosensors since it is a useful tool to evaluate the interactions between biomolecules. In this context, this technique has found diverse applications in distinct fields due to its sensitivity and effectivity for analyzing interfacial phenomena in modified electrodes, essentially becoming an excellent alternative to traditional methods of diagnosis [10,11]. Compared to other techniques, one of the advantages of EIS is that it provides information about electrode kinetics and the electrical double layer. Cyclic voltammetry (CV) is a method that provides the interface information of a biologically modified electrode, enabling monitoring of the rate of charge transfer between the electrode and the solution [12]. Electrochemical techniques have been extensively used to characterize the development of biosensors and to evaluate biomolecular recognition [13,14].

* Corresponding author at: Departamento de Bioquímica, Universidade Federal de Pernambuco, 50670-901 Recife, PE, Brazil. Fax: +55 81 2126 8547.
E-mail address: m_danielly@yahoo.com.br (M.D.L. Oliveira).

http://dx.doi.org/10.1016/j.jcis.2014.07.014
0021-9797/

Metal oxide nanoparticles exhibit unique properties, such as increased surface area, magnetism, chemical reduction, ligand sequestration and optical characteristics [15–17]. In general, magnetic nanoparticles have advantages such as good susceptibility, dispersibility and the ability to be used in association with other metal nanoparticles to obtain new properties without change in its magnetic properties [18,19]. In addition, magnetic nanoparticles covered by a thin gold layer have been used for isolation, purification or detection of genomic DNA [20]. In addition, magnetite nanoparticles (Fe_3O_4Nps) offer a versatile tool for the development of DNA-based electrochemical sensors [21]. The use of nanotechnology for the development of genosensors has attracted attention due to potential applications in forensic identification, epidemic prevention and disease diagnosis [22].

Self-assembled monolayers (SAMs) have been extensively used in derivatization procedures to obtain versatile modified surfaces, offering a molecular dimension with organization and homogeneity [23,24]. Metal surfaces can be modified using SAMs based on organic molecules that contain anchor groups such as thiols, disulfides, silanes or acids to enhance the biomolecular stability. Mercaptobenzoic acid (MBA) has an SH sulfhydryl functional group that interacts with metal surfaces and a carboxylic acid group available for covalent interaction with nanostructures and biomolecules. In this point of view, nanostructured sensors are an excellent alternative for new methods of diagnosis since they are rapid, inexpensive, sensitive and present accurate identification [25,26].

In the present study, we developed a sensitive nanostructured layer based on DNA probes chemically attached to Fe_3O_4Nps that can be used for monitoring the hybridization of TB DNA. The proposed sensor requires the use of small volumes and low concentrations of analyte. Amino functionalized Fe_3O_4NPs were bound to the self-assembled monolayer of the MBA through 1-ethyl-3-(3-dimethylaminopropyl) carbodiimide and N-hydroxysuccinimide (EDC/NHS) coupling. After that, 5′-amino modified DNA probes were chemically bound to the Fe_3O_4Nps–MBA-modified electrode using the EDC/NHS coupling method. The modification of Fe_3O_4Nps with aminated groups was important to provide covalent linkage between COOH MBA groups and NH_2–Fe_3O_4Nps. This assembly enabled electrode surface modification to receive the biological sample in study. In addition, this coverage of the electrode is an efficient maintenance tool for the biological structure. Finally, the obtained sensor system was used for specific detection of the genetic material of patients contaminated with *M. tuberculosis*. To the best of our knowledge, this is the first report about TB diagnosis using Fe_3O_4Nps and MBA self-assembled monolayers (SAMs). An overview of the fabrication process of the biosensor is shown in Fig. 1. The assembly process and sensor assays were characterized by CV, EIS and atomic force microscopy.

2. Experimental

2.1. Materials

Ferric chloride, ferrous chloride, potassium ferri- and ferrocyanide were obtained from VETEC (Brazil). 3-Aminopropyltriethoxysilane (APTS) and MBA were purchased from Sigma–Aldrich (St. Louis, USA). All chemicals and solvents were of analytical grade and used as received, without further purification. Water used was obtained from a Milli-Q plus (Billerica, USA) purification system. TB samples were obtained from the stocks at the Laboratory of Parasitology at Aggeu Magalhaes Research Center (Recife, Brazil). All samples were previously characterized using RT-qPCR. The sequence for the amine-modified DNA probes used for the development of the biosensor was 5′-TCAGGGGATGGGGCCTAG-3′ [27].

2.2. Synthesis and chemical modification of Fe_3O_4Nps

Magnetite nanoparticles were synthesized using the coprecipitation method of Fe^{3+} and Fe^{2+} [28]. 0.1 M $FeCl_3{\cdot}6H_2O$ and 0.5 M $FeSO_4{\cdot}7H_2O$ were mixed in 200 mL of water under stirring for 30 min under N_2 atmosphere. Subsequently, a 1.5 M NH_4OH aqueous solution was added into the resulting mixture dropwise until the liquid turned blackish, and was left under stirring overnight at room temperature. The synthesized magnetite particles were separated using magnetic field. NH_2-modified Fe_3O_4Nps were obtained according to the literature [29]. First, 0.2 g magnetite particles were dispersed in 90 mL of ethanol (50%) using an ultrasonic bath. Afterward, 300 μL APTES and 500 μL NH_4OH were added dropwise to the previous solution. The resulting solution was heated to 60 °C under a stream of nitrogen for 6 h with vigorous agitation.

2.3. Immobilization of TB DNA probe and hybridization with genomic DNA target

The bare gold disk electrode (BGE) with ϕ = 2 mm (Microchimica, Brazil) was polished with alumina powder (0.05 μm), sonicated in ultrapure water (18 MΩ cm^{-1}) for 10 min and air dried. Afterward, 2 μL MBA (5%) was dropped on the electrode surface until dry to obtain MBA SAMs on gold surface. The carboxylic groups presented in the MBA molecules were activated using an aqueous solution containing 0.4 mmol L^{-1} EDC and 0.1 mmol L^{-1} NHS (1:1 v/v) for 20 min. Subsequently, the electrode was washed and 2 μL Fe_3O_4Nps was dropped on the MBA–EDC/NHS-modified electrode, waiting 10 min to obtain the MBA–EDC/NHS–Fe_3O_4NPs system. Then, MBA–EDC/NHS–Fe_3O_4NPs-modified electrode was activated with glutaraldehyde to allow the immobilization of DNA $probe_{tuberculosis}$, incubated for 30 min and washed with phosphate buffered saline (PBS). In addition, the specificity of the AMB–Fe_3O_4Nps–DNA-$probe_{tuberculosis}$-modified electrode was evaluated against genomic DNA target (Fig. 1) at different incubation times (1, 10, 20 and 30 min).

2.4. Electrochemical measurements

Electrochemical data was obtained by a PGSTAT 128N potentiostat/galvanostat (Autolab, Eco-Chemie, Netherlands) interfaced with an analyzer controlled by a computer. The experiments were performed using a three-electrode system in a conventional cell composed by a BGE platinum electrode and Ag/AgCl saturated with KCl as working, counter and reference electrodes, respectively. 10 mM $[Fe(CN)_6]^{4-}$/$[Fe(CN)_6]^{3-}$ (1:1) solution containing 0.15 M NaCl was used as a redox probe in PBS (pH 7.4). CV measurements were performed at potential range between +0.7 V and −0.2 V at a scan rate of 50 mV s^{-1}. EIS frequency ranges were between 100 mHz to 100 kHz with amplitude of the applied sine wave potential of 10 mV. Electrochemical measurements were carried out at room temperature and inside a Faraday cage. All experiments were performed in triplicate using at least three different sensors.

2.5. Atomic force microscopy measurements

Structural analysis of the sensor was performed by an atomic force microscope (Agilent AFM, Picoplus Molecular Imaging, USA) [7]. Cantilevers with a silicon AFM probe (Multi 75AL, NCHR, resonant frequency = 75 kHz, force constant = 3 N m^{-1}) were used for the noncontact mode AFM in air at room temperature (approximately 25 °C). Lateral resolution was set to 512 × 512 pixels in a scan area of 5 × 5 μm. To eliminate artifacts, images were obtained

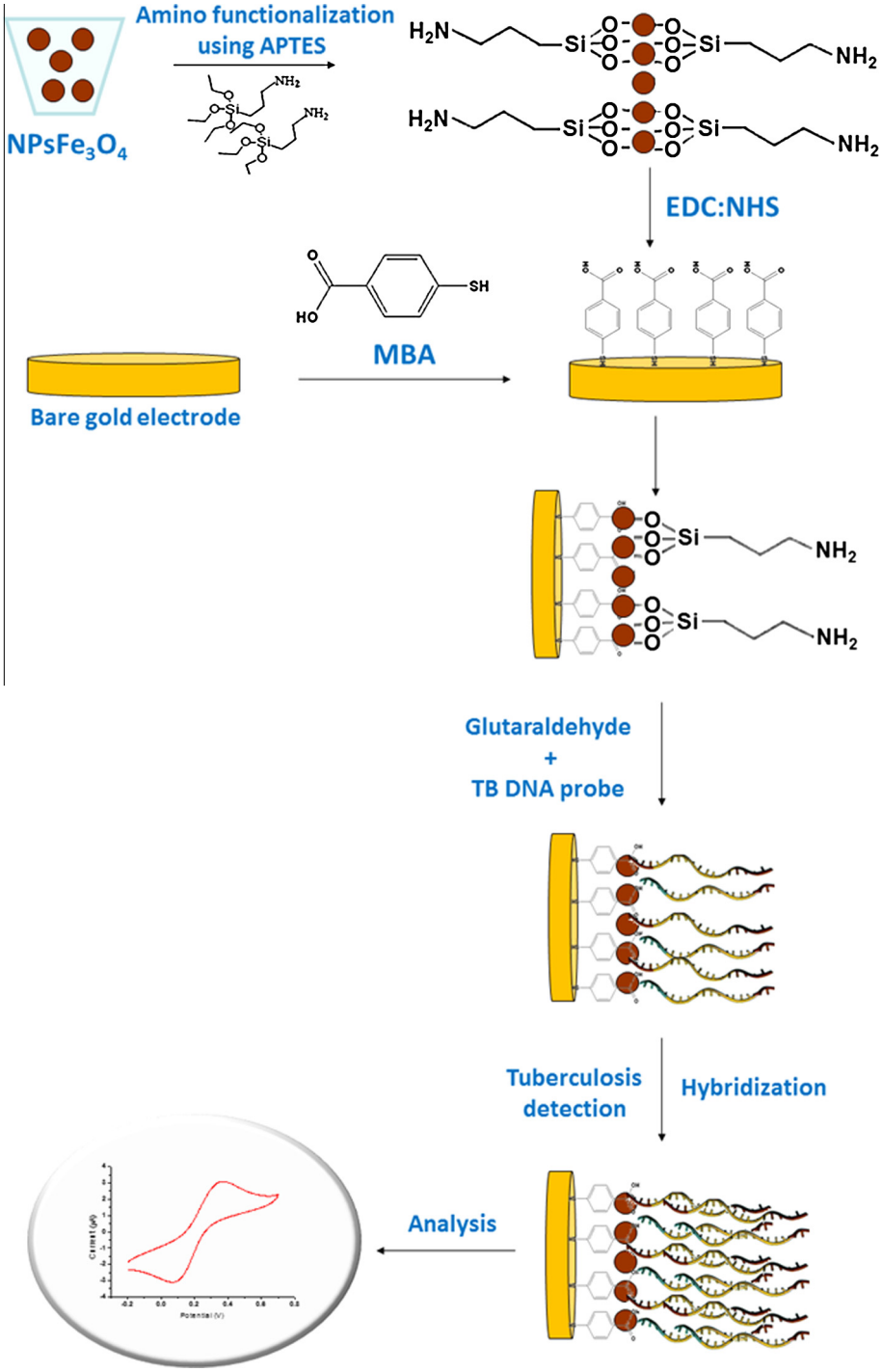

Fig. 1. Schematic representation of the fabrication process of the biosensor.

from at least two macroscopically-separated areas on each sample and analyzed using AFM Gwyddion software [30].

3. Results and discussion

3.1. Morphological analyses

Atomic force microscopy was used to confirm the self-assembled process of the biosensor construction and investigate the changes of the surface morphology of the sensor system before and after interaction with TB genomic DNA samples. After the adsorption of the Fe_3O_4Nps nanoparticles on the solid substrate surface, the smooth surface morphology of the clean substrate was modified due to the presence of dispersed particles (Fig. 2a). It was observed that the small particles had z-average diameter values of 15 ± 1.7 nm, similar to previous studies [31]. In sequence, the interaction of the Fe_3O_4Nps with the oligonucleotide sequence resulted in the increase of the surface roughness (Fig. 2b) and z-average diameter values of 21 ± 2.2 nm. The difference of ~6 nm corresponded to the height of oligonucleotides comprised by 18 bases [32]. Of note, amino groups on the surface of the Fe_3O_4Nps were used not only as covalently linked groups, but also as protective groups [33].

The specific interaction with samples from patients contaminated with TB resulted in a dramatic change in the morphology and heterogeneous surface with the presence of some peaks, indicating that the TB sample was successfully recognized on the sensor surface (Fig. 2c). On the other hand, Fig. 2d shows the morphology for a non-complementary target where there were no significant changes on the sensor surface. Therefore, our results confirm the specificity of the sensor, since the nonspecific adsorption on the DNA modified-biosensor surface was not significant.

3.2. Electrochemical characterization

CV is an effective method for providing information for the changes in electrode behavior after each step of modification, since the changes in peak current and the separation of peak potentials are related to electron transfer resistance [6]. Each step of surface modification was monitored by CV using a $Fe(CN)_6^{3-}/Fe(CN)_6^{4-}$ solution containing 0.15 M NaCl in PBS (pH 7.4) as a redox probe (see Fig. 2).

CV and EIS spectra of the stepwise electrode surface modification are shown in Fig. 3. As shown in Fig. 3a, the redox probe $Fe(CN)_6^{3-}/Fe(CN)_6^{4-}$ revealed a reversible cyclic voltammogram for the gold electrode. A decrease in the current response was observed after the modification of BGE by MBA, due to the repulsion effect between the negative charges of MBA and the redox pair. MBA SAMs are an excellent alternative to enhance the genosensor performance due to the presence of the aromatic ring [34]. In addition, the carboxylic group can be used for the covalent linkage of biomolecules and act as an anchor for interfacing the modified magnetic nanoparticle [34,35]. Previously, some authors [36] reported no difference in electrode surface coverage using MBA after a prolonged adsorption time due to the formation of stable and ordered MBA films. In addition, the presence of aromatic thiols can lead to the establishment of π-stacking [37]. Metal nanoparticles, such as Fe_3O_4Nps, can be oxidized or reduced electrochemically resulting in enhanced sensitivity of the biosensor [38]. Voltammograms have demonstrated a quasi-reversible behavior after the presence of Fe_3O_4Nps–MBA at the electrode surface when compared with cleaned electrode. Subsequently, the electrode was activated by the co-addition of NHS and EDC coupling agents.

The negatively charged terminal carboxylic group of MBA was replaced by NHS ester. Thus, the carboxylic group replacement contributed to the electrostatic attraction between the neutrally/positively charged NHS ester and the negative redox probe resulting in increased current response [39]. The amperometric response decreases after the binding of Fe_3O_4Nps to MBA monolayers, since the penetration of the redox probe is reduced. This modification decreased the current peaks and the presence of Fe_3O_4Nps at electrode surface, promoting a biocompatible layer for biosensor development. In addition, after the DNA probe immobilization and DNA target hybridization, the anodic and cathodic peaks were reduced. The decrease in the amperometric response of the sensor system was attributed to the blocking effect of biomolecular recognition that reduces the electron transfer of the redox pair (Fig. 3a).

EIS can provide further information for the impedance changes during the modification process and is an effective way to measure to electron transfer resistance (R_{CT}) [8]. R_{CT} corresponds to the semicircle diameter of the Nyquist diagram. EIS was carried out to characterize the assembly process on the BGE surface in the frequency range of 100 mHz to 100 kHz.

Complex impedance plots of BGE and stepwise electrode modification are shown in Fig. 3a. Fig. 3b shows the Nyquist plots for each step of assembly. Cole–Cole semicircle is composed by two well-defined regions at higher and lower frequencies, corresponding to the electron transfer-limited and diffusion-limited electron transfer processes, respectively. The MBA impedimetric response showed greater interfacial electron transfer resistance (R_{CT} = 175 - kΩ), indicating that the adsorbed layer obstructed the electron transfer of the electrochemical probe. The modification of the MBA layer using NHS/EDC coupling agents resulted in a decrease of the R_{CT} (R_{CT} = 14.50 kΩ). After the immobilization of the Fe_3O_4-Nps on AMB-modified electrode an increased in the R_{CT} = 29.50 kΩ was obtained. As expected, after the coupling of Fe_3O_4Nps–AMB-modified electrode with DNA $probe_{tuberculosis}$, the interfacial resistance increased remarkably (R_{CT} = 168.0 kΩ). EIS data indicated the presence of molecules at the electrode surface, where the amount of material immobilized and adsorbed reflected the increase in impedance response. Furthermore, the layers were successfully assembled on the BGE surface.

In addition, the time of incubation and hybridization have an important role for the performance of biosensor. Of note, the incubation period is involved in the rate of available molecules for biomolecular recognition. A detailed study to determine the incubation time was carried out (Fig. 3c). In our study, the increased time of incubation resulted in an increase in the electrochemical response. Estimates of the best response were based on tendency of plateau of the R_{CT} of DNA $probe_{tuberculosis}$ versus time of incubation.

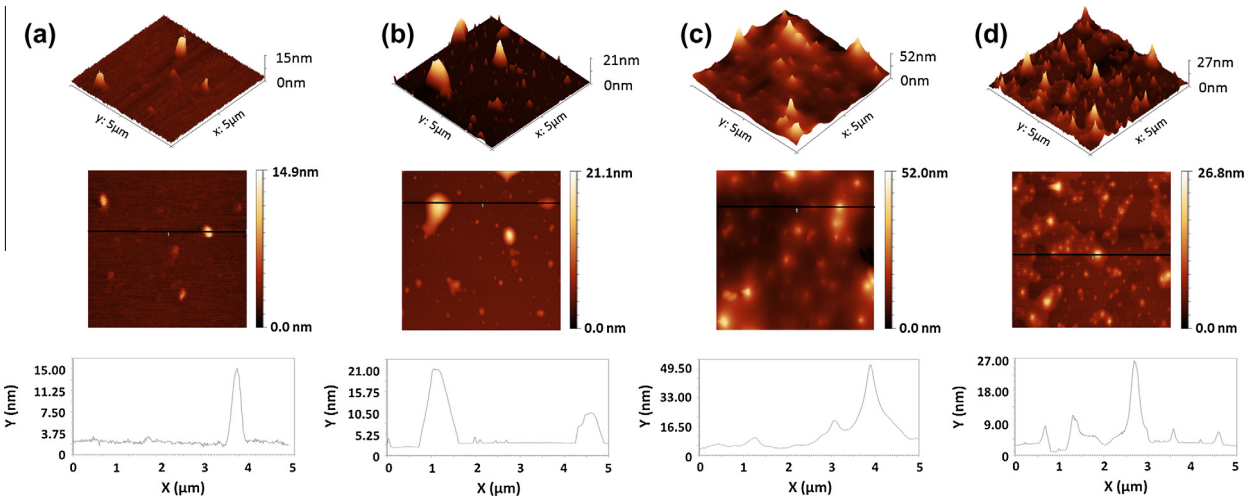

Fig. 2. 3D and 2D AFM images of the BGE coated with Fe_3O_4Nps (a), Fe_3O_4Nps–probe (b), MBA–Fe_3O_4Nps–DNA-probe-complementary DNA (c) and MBA–Fe_3O_4Nps–DNA-probe non-complementary DNA (d), with the corresponding cross section.

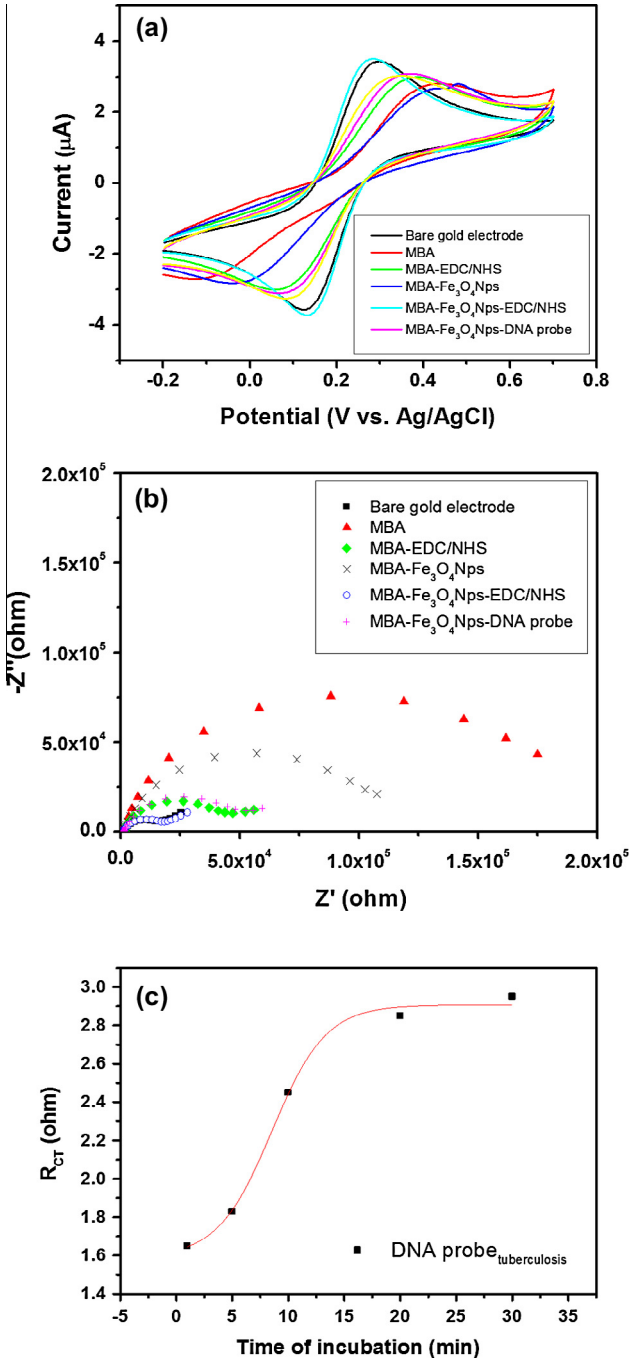

Fig. 3. Cyclic voltammograms (a) and Nyquist plots (b) of the stepwise immobilization of the MBA–Fe_3O_4Nps–DNA-probe: bare gold electrode (■), MBA-modified gold electrode (▲), MBA–EDC/NHS (♦), MBA–Fe_3O_4Nps (×), MBA–Fe_3O_4Nps–EDC/NHS (○) and MBA–Fe_3O_4Nps–DNA-probe (+). R_{CT} of DNA probe-tuberculosis versus time of incubation (c). The impedance spectra were taken in 10 mM $[Fe(CN)_6]^{4-}$/$[Fe(CN)_6]^{3-}$ 1:1 + 0.15 M NaCl in 10 mM PBS (pH 7.4) in the frequency range from 100 mHz to 100 kHz.

3.3. Detection of TB genomic DNA target

Fig. 4 shows the representative voltammograms and Nyquist diagrams of the genosensor exposed to different concentrations of TB genomic DNA target. Fig. 4a shows the CVs for the sensor system at different concentrations of genomic DNA target. After the modification of the electrode surface and the DNA target recognition process, a decrease was observed in the CV peaks of the redox probe followed by an increase in the peak-to-peak separation (Fig. 4a). The extent of adsorption can be expressed in a relative percent deviation (RPD),

$$I(\%) = \frac{[(1/Ib) - (1/Ia)}{(1/Ib)} \quad (1)$$

where *Ib* and *Ia* correspond to the anodic peak current before and after the hybridization process, respectively. Table 1 shows the result of RPD for the MBA–Fe_3O_4Nps–DNA-probe-modified electrode before and after the reaction with different concentrations of DNA target.

A more detailed study was carried out for different TB genomic DNA target concentrations, demonstrating that specific DNA interaction can be quantitatively assessed by the sensor (Fig. 4b and d). Curves d–h (Fig. 4b) represent the concentration of TB genomic DNA target (6, 12, 20, 30 and 40 ng μL^{-1}). R_{CT} increased along with the increase of TB DNA target concentration as shown in curves d–h (Fig. 4b).

The electrochemical impedance diagrams (Nyquist plots) were subjected to an analysis of data through EQUIVCRT[40], from which theoretical curves were obtained for each system as a valuable tool to explore the interfacial behavior of the sensor system in the recognition of TB DNA target sequences. The experimental spectra were fitted using a modified Randles equivalent circuit (Fig. 4c). Warburg impedance (Z_W) represents the impedance of semi-infinite diffusion of the redox probe to the electrode. The ohmic resistance of the solution (R_Ω) is associated with the bulk properties of the electrolyte solution. Constant-phase element (Q) represents the behavior of a double layer for a non-homogeneous system. Electron transfer resistance (R_{CT}) is related to the dielectric features of a material to charge transport.

The Bode plot demonstrates three types of elements of the equivalent circuit (Fig. 4d). At the low frequency range the response of the double layer capacitance represented by the phase constant element was observed. A frequency region below 3 kHz corresponded to R_{CT} and the region above 20 kHz was related to solution resistance. In this context, in the capacitance region of frequency negligible changes in Q values were obtained during the hybridization process at different concentrations of genomic DNA target, showing a non-capacitive behavior of the bioelectrode. MBA–Fe_3O_4Nps–DNA-probe modified electrode showed a well-defined concentration-dependence curve for the TB genome interaction.

The obtained results demonstrated that the biosensor retained the capability to recognize the specific DNA target (Table 2). The performance of the biosensor for detection of TB genomic DNA target was evaluated through the relative variation of the R_{CT} (ΔR_{CT}), according to the equation:

$$\Delta R_{CT}\ (\%) = \frac{R_{CT(recog)} - R_{CT(sensor)}}{R_{CT(sensor)}} \quad (2)$$

where $R_{CT(recog)}$ is the value of the electron-transfer resistance after the DNA target recognition, and $R_{CT(sensor)}$ corresponds to the R_{CT} value of the sensor layer. Sensitivity analysis for TB genomic DNA target was evaluated from the ΔR_{CT} results.

A linear relationship between the ΔR_{CT} and DNA target concentration was found (Fig. 5a) with the correlation coefficient of 0.98, indicating that the interactions between probe and DNA target can be sensed by the modified electrode. The detection limit of 6 ng μL^{-1} was estimated from the signal-to-noise characteristics of these data (S/N = 3). The signal-to-noise ratio was obtained from the impedimetric variation divided by the standard deviation [41]. The increase in ΔR_{CT} seemed to present a profile of saturation (Fig. 5a). Our detection limits were similar to previous reports that

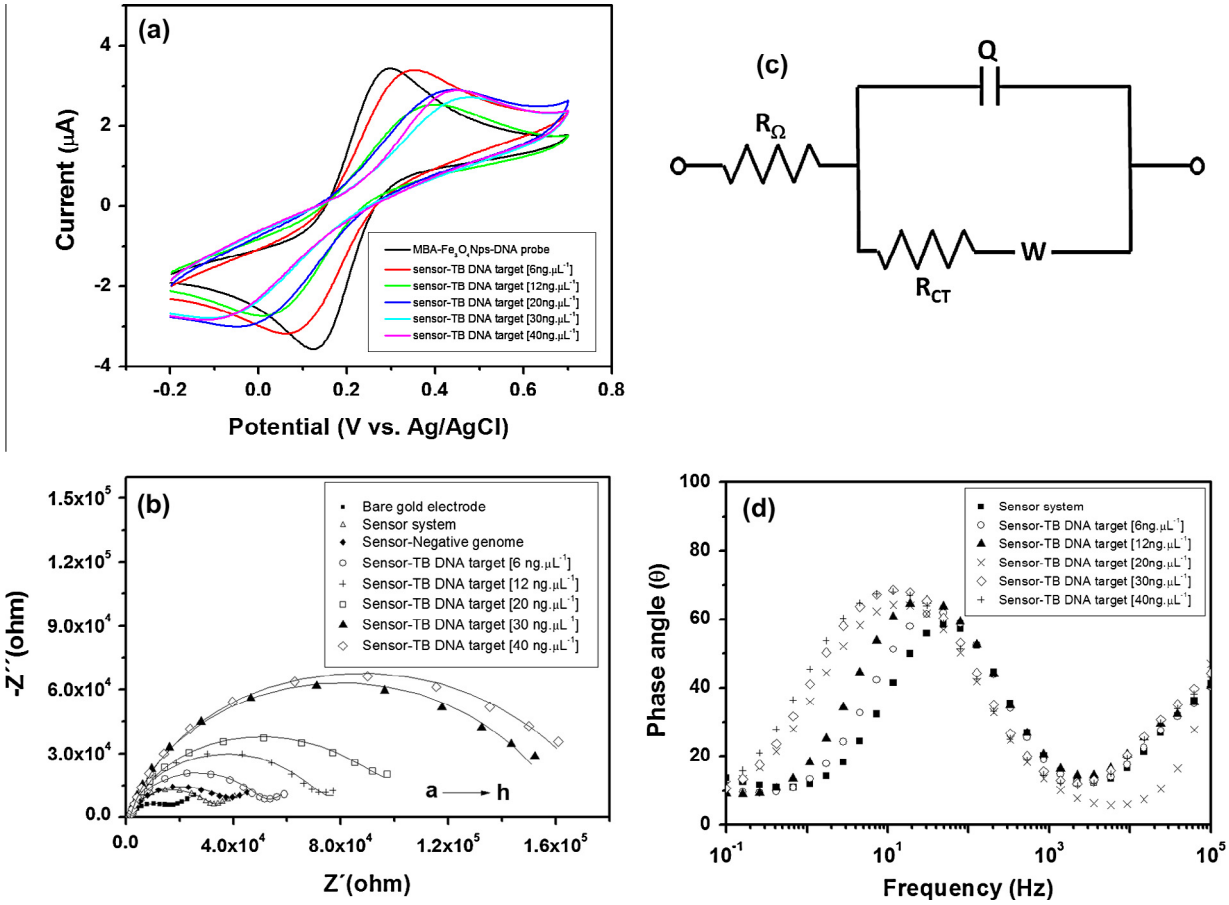

Fig. 4. Cyclic voltammograms (a), Nyquist plots (b) and Bode plots (d) of the sensor system and its respective interaction with genomic DNA target at different concentrations. Supporting electrolyte: 10 mM $[Fe(CN)_6]^{4-}/[Fe(CN)_6]^{3-}$ 1:1 + 0.15 M NaCl in 10 mM PBS (pH 7.4) solution; scan rate of 50 mV s^{-1}. Equivalent circuit (c) adopted to fit the impedance data where R_Ω is the ohmic resistance of the electrolyte solution, Q the phase constant element, Z_W the Warburg impedance, and R_{CT} the electron-transfer resistance.

Table 1
Amperometric anodic shift for the sensor before and after the hybridization with TB genomic DNA target.

Sample[a]	TB DNA target (ng μL^{-1})	Before ($1/Ib$ μA)	After	ΔI (%)
Sensor system	–	0.312	–	–
Sensor system-TB genomic DNA target	6	–	0.482	54.48
Sensor system-TB genomic DNA target	12	–	0.518	66.02
Sensor system-TB genomic DNA target	20	–	0.613	96.47
Sensor system-TB genomic DNA target	30	–	0.621	99.03
Sensor system-TB genomic DNA target	40	–	0.735	135.50

[a] Sensor system = AMB–Fe_3O_4Nps–DNA $probe_{tuberculosis}$.

Table 2
Values of the equivalent circuit elements from fitted impedance results.

Modified electrode	TB DNA target (ng μL^{-1})	R_{CT} (kΩ)	Q (μF)	N
Bare gold electrode	–	15.30 ± 0.21	3.20 ± 0.33	0.82 ± 0.05
AMB–Fe_3O_4Nps–DNA $probe_{tuberculosis}$	–	29.50 ± 0.30	0.82 ± 0.02	0.89 ± 0.03
Sensor system-TB genomic DNA target	6	47.90 ± 0.40	0.77 ± 0.17	0.89 ± 0.09
Sensor system-TB genomic DNA target	12	70.00 ± 0.13	0.93 ± 0.02	0.88 ± 0.04
Sensor system-TB genomic DNA target	20	92.90 ± 0.22	1.92 ± 0.11	0.85 ± 0.02
Sensor system-TB genomic DNA target	30	154.0 ± 0.34	1.44 ± 0.30	0.86 ± 0.02
Sensor system-TB genomic DNA target	40	168.0 ± 0.65	1.66 ± 0.80	0.85 ± 0.04
Sensor system-non complementary DNA target	–	15.30 ± 0.15	1.88 ± 0.44	0.84 ± 0.04

Sensor system = AMB–Fe_3O_4Nps–DNA $probe_{tuberculosis}$.

used electrochemical techniques for the specific detection of the TB DNA target [42,43]. However, these reports had limitations based on the identification of only a small tuberculosis-specific DNA fragment [42] or necessity of $Co(phen)_3^{3+}$ indicator binding to the biorecognition analysis [43]. On the other hand, gold nanoparticles associated with nucleotide probes have been used in colorimetric assays to identify TB DNA with a detection limit of 18.75 ng μL^{-1} [44], but the cost per test corresponds to ~70–120% of RT-PCR.

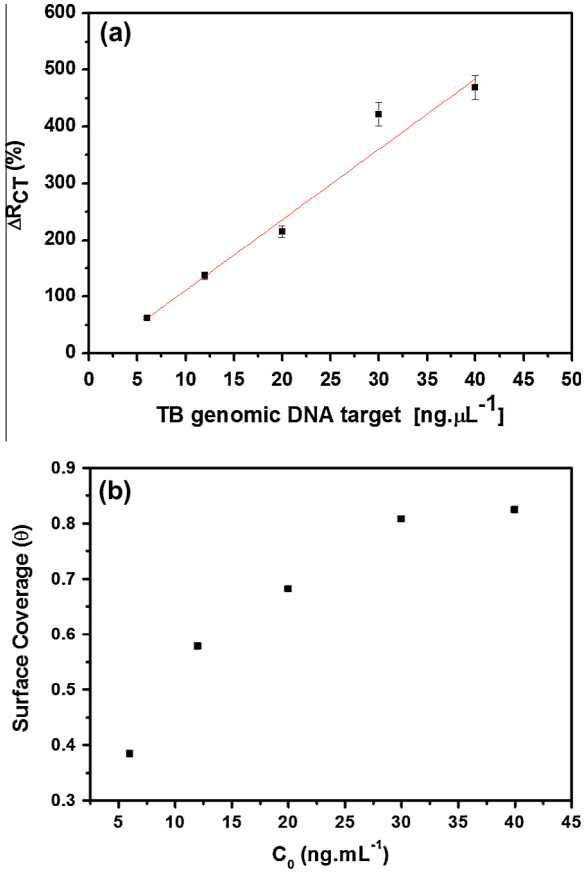

Fig. 5. ΔR_{CT}% of the sensor system after exposure to different concentrations of TB genomic DNA target (a) and θ as a function of concentration of DNA target (b).

We can observe that the filling of the recognition sites by DNA target surface coverage (θ) can be calculated by:

$$\theta = \frac{1 - R_B}{R_C} \quad (3)$$

where R_B is the charge transfer resistance for MBA–Fe_3O_4Nps–DNA-probe biosystem and R_C is the charge transfer resistance obtained for different concentrations of the TB DNA target hybridized with the biosensor. Fig. 5b shows a plot of θ as a function of concentration of DNA target bound to the sensor. The value of θ increases with increasing DNA-target concentration and is found to be ~0.82 (82%) of the 40 ng mL^{-1} DNA target.

A regeneration study was performed by exposing the sensor to a 100 μL alkaline solution (0.5 M NaOH with 3 M NaCl) for 20 min [45]. Of note. extra time for the dehybridization experiments was necessary as compared to hybridization study, since it is necessary disrupt the DNA base-stacking interactions [46]. The biosensor can be regenerated for five cycles, allowing reuse until its loss of hybridization capacity. The results revealed a relative standard deviation (R.S.D.) of 1.32%, $n = 3$.

In addition, selectivity is a crucial factor to be considered for DNA sensors. The selectivity of the biosensor was investigated by monitoring changes in the R_{CT} response by incubating with complementary and non-complementary DNA sequences (Fig. 4c, curve c). We used non-complementary genomic DNA from Leishmaniasis as a negative control. The interaction of the biosensor with a non-complementary DNA sequence (negative control) resulted in an insignificant R_{CT} value, revealing the selectivity of the bioelectrode. The reproducibility of the DNA sensor using at least three DNA sensors fabricated independently at the same conditions was evaluated. An acceptable R.S.D. of ~5% was obtained, suggesting that the DNA sensor is reproducible. Our results indicate the applicability of the MBA–Fe_3O_4Nps layer as an excellent matrix to immobilize biomolecules for the development of a useful biosensor for tuberculosis using small volumes of samples.

4. Conclusions

The impedimetric response demonstrates the success of the modification process on the electrode surface. The TB DNA sensor showed an increased impedimetric response to increasing target DNA concentrations. The sensitivity of the biosensor for TB genomic DNA target was 6 ng μL^{-1}. The biosensor showed acceptable performances for the determination of TB DNA target, exhibiting low detection limit, selectivity and reproducibility in the DNA hybridization assay. The proposed biosensor has advantages such as operation convenience, capability of analyzing small quantities of biological material within minutes and the possibility for use in a miniaturized format. We believe that the present results are an important basis for the development of sensitive DNA sensors and a useful strategy for tuberculosis diagnosis using clinical samples.

Acknowledgments

The authors are grateful for the support provided by FACEPE, CNPq and Rede de Nanobiotecnologia/CAPES. Andrade and Oliveira are also gratefully for the financial support from CNPq (Grant 310305/2012-8 and 310361/2012-5, respectively). M.P. Palmeira would like to thank FACEPE for a M.Sc. scholarship.

References

[1] N. Prabhakar, K. Arora, S.K. Arya, P.R. Solanki, M. Iwamoto, H. Singh, B.D. Malhotra, Analyst 133 (2008) 1587.
[2] K.L. Kaul, Clin. Chem. 47 (2001) 1553.
[3] M. Koziol-Montewka, A. Kolodziejek, J. Oles, L. Janicka, Immunol. Invest. 33 (2004) 277.
[4] C.P. Wang, X.Q. Yuan, X.H. Liu, Q. Gao, H.L. Qi, C.X. Zhang, Anal. Chim. Acta 799 (2013) 36.
[5] J.Y. Park, S.M. Park, Sensors 9 (2009) 9513.
[6] M.D.L. Oliveira, D.S.P. Abdalla, D.F. Guilherme, T.E.S. Faulin, C.A.S. Andrade, Sens. Actuators, B – Chem. 155 (2011) 775.
[7] M.D.L. Oliveira, C.A.S. Andrade, M.T.S. Correia, L.C.B.B. Coelho, P.R. Singh, X.Q. Zeng, J. Colloid Interface Sci. 362 (2011) 194.
[8] M.D.L. Oliveira, M.L. Nogueira, M.T.S. Correia, L.C.B.B. Coelho, C.A.S. Andrade, Sens. Actuators, B – Chem. 155 (2011) 789.
[9] A.B. Kharitonov, L. Alfonta, E. Katz, I. Willner, J. Electroanal. Chem. 487 (2000) 133.
[10] Y.X. Hou, S. Helali, A.D. Zhang, N. Jaffrezic-Renault, C. Martelet, J. Minic, T. Gorojankina, M.A. Persuy, E. Pajot-Augy, R. Salesse, F. Bessueille, J. Samitier, A. Errachid, V. Akimov, L. Reggiani, C. Pennetta, E. Alfinito, Biosens. Bioelectron. 21 (2006) 1393.
[11] I. Navratilova, P. Skladal, Bioelectrochemistry 62 (2004) 11.
[12] A.J. Bard, L.R. Faulkner, Electrochemical Methods: Fundamentals and Applications, second ed., John Wiley & Sons, New York, 2000.
[13] J.G. Guan, Y.Q. Miao, Q.J. Zhang, J. Biosci. Bioeng. 97 (2004) 219.
[14] E. Katz, I. Willner, Electroanalysis 15 (2003) 913.
[15] S. Sarkar, E. Guibal, F. Quignard, A.K. SenGupta, J. Nanopart. Res. 14 (2012) 715.
[16] K. Pospiskova, I. Safarik, M. Sebela, G. Kuncova, Microchim. Acta 180 (2013) 311.
[17] E. Katz, I. Willner, Angew. Chem., Int. Ed. 43 (2004) 6042.
[18] P. Tartaj, M.D. Morales, S. Veintemillas-Verdaguer, T. Gonzalez-Carreno, C.J. Serna, J. Phys. D: Appl. Phys. 36 (2003) R182.
[19] M. Pita, J.M. Abad, C. Vaz-Dominguez, C. Briones, E. Mateo-Marti, J.A. Martin-Gago, M.D.P. Morales, V.M. Fernandez, J. Colloid Interface Sci. 321 (2008) 484.
[20] H.D. Hill, R.A. Vega, C.A. Mirkin, Anal. Chem. 79 (2007) 9218.
[21] K. Li, Y.J. Lai, W. Zhang, L.T. Jin, Talanta 84 (2011) 607.
[22] Q.R. Zhang, P.P. Dai, Z.S. Yang, Microchim. Acta 173 (2011) 347.
[23] A. Ulman, An Introduction to Ultrathin Organic Films from Langmuir–Blodgett to Self-Assembly, Academic Press, New York, 1991.
[24] J.D. Swalen, D.L. Allara, J.D. Andrade, E.A. Chandross, S. Garoff, J. Israelachvili, T.J. Mccarthy, R. Murray, R.F. Pease, J.F. Rabolt, K.J. Wynne, H. Yu, Langmuir 3 (1987) 932.

[25] W. Wang, L.N. Song, Q. Gao, H.L. Qi, C.X. Zhang, Electrochem. Commun. 34 (2013) 18.
[26] Y. Zhang, K. Zhang, H. Ma, Am. J. Biomed. Sci. 1 (2009) 115.
[27] L.E. Desjardin, M.D. Perkins, K. Wolski, S. Haun, L. Teixeira, Y. Chen, J.L. Johnson, J.J. Ellner, R. Dietze, J. Bates, M.D. Cave, K.D. Eisenach, Am. J. Respir. Crit. Care 160 (1999) 203.
[28] H.P. de Oliveira, C.A.S. Andrade, C.P. de Melo, J. Colloid Interface Sci. 319 (2008) 441.
[29] N. Gan, H.J. Jin, T.H. Li, L. Zheng, Int. J. Nanomed. 6 (2011) 3259.
[30] D. Necas, P. Klapetek, C. Anderson, Gwyddion, 2008. <http://www.gwyddion.net>.
[31] M. Yamaura, R.L. Camilo, L.C. Sampaio, M.A. Macedo, M. Nakamura, H.E. Toma, J. Magn. Magn. Mater. 279 (2004) 210.
[32] Z.L. Zhang, D.W. Pang, H. Yuan, R.X. Cai, H. Abruna, Anal. Bioanal. Chem. 381 (2005) 833.
[33] Z.X. Zhang, X.L. Wang, X.R. Yang, Analyst 136 (2011) 4960.
[34] H. Wang, H. Ohnuki, H. Endo, M. Izumi, Phys. Proc. 14 (2011) 2.
[35] R.G. Nuzzo, L.H. Dubois, D.L. Allara, J. Am. Chem. Soc. 112 (1990) 558.
[36] Y. Jalit, F.A. Gutierrez, G. Dubacheva, C. Goyer, L. Coche-Guerente, E. Defrancq, P. Labbe, G.A. Rivas, M.C. Rodriguez, Biosens. Bioelectron. 41 (2013) 424.
[37] J.C. Love, L.A. Estroff, J.K. Kriebel, R.G. Nuzzo, G.M. Whitesides, Chem. Rev. 105 (2005) 1103.
[38] L. Ding, A.M. Bond, J.P. Zhai, J. Zhang, Anal. Chim. Acta 797 (2013) 1.
[39] P. Geng, X. Zhang, W. Meng, Q. Wang, W. Zhang, L. Jin, Z. Feng, Z. Wu, Electrochim. Acta 53 (2008) 4663.
[40] B.A. Boukamp, Solid State Ionics 18–9 (1986) 136.
[41] N. Couniot, D. Flandre, L.A. Francis, A. Afzalian, Sens. Actuators, B – Chem. 189 (2013) 43.
[42] E. Torres-Chavolla, E.C. Alocilja, Biosens. Bioelectron. 26 (2011) 4614.
[43] J. Wang, G. Rivas, X.H. Cai, N. Dontha, H. Shiraishi, D.B. Luo, F.S. Valera, Anal. Chim. Acta 337 (1997) 41.
[44] E. Liandris, M. Gazouli, M. Andreadou, M. Comor, N. Abazovic, L.A. Sechi, J. Ikonomopoulos, J. Microbiol. Methods 78 (2009) 260.
[45] M. Lazerges, H. Perrot, N. Zeghib, E. Antoine, C. Compere, Sens. Actuators, B – Chem. 120 (2006) 329.
[46] A.V. Ladik, F.M. Geiger, S.R. Walter, Nanoscape 7 (2010) 19.